Please cite as:
Watanabe et al. (2019), “Hayabusa2 arrives at the carbonaceous asteroid 162173 Ryugu—A spinning top–shaped rubble pile”, Science, Vol. 364, pp. 268-272,
doi: https://doi.org/10.1126/science.aav8032

Title: Hayabusa2 observations of the top-shaped carbonaceous asteroid 162173 Ryugu

Short title: Hayabusa2 observations of asteroid Ryugu

Authors: S. Watanabe[1,2]*, M. Hirabayashi[3], N. Hirata[4], N. Hirata[5], R. Noguchi[2], Y. Shimaki[2], H. Ikeda[6], E. Tatsumi[7], M. Yoshikawa[2], S. Kikuchi[2], H. Yabuta[8], T. Nakamura[9], S. Tachibana[7,2], Y. Ishihara[2†], T. Morota[1], K. Kitazato[4], N. Sakatani[2], K. Matsumoto[10,11], K. Wada[12], H. Senshu[12], C. Honda[4], T. Michikami[13], H. Takeuchi[2], T. Kouyama[14], R. Honda[15], S. Kameda[16], T. Fuse[17], H. Miyamoto[7], G. Komatsu[18,12], S. Sugita[7], T. Okada[2], N. Namiki[10,11], M. Arakawa[5], M. Ishiguro[19], M. Abe[2], R. Gaskell[20], E. Palmer[20], O. S. Barnouin[21], P. Michel[22], A. S. French[23], J. W. McMahon[23], D. J. Scheeres[23], P. A. Abell[24], Y. Yamamoto[2], S. Tanaka[2], K. Shirai[2], M. Matsuoka,[2] M. Yamada,[12] Y. Yokota,[2] H. Suzuki,[25] K. Yoshioka,[7] Y. Cho,[7] S. Tanaka,[5] N. Nishikawa[5], T. Sugiyama[4], H. Kikuchi[7], R. Hemmi[7], T. Yamaguchi[2††], N. Ogawa[2], G. Ono[6], Y. Mimasu[2], K. Yoshikawa[6], T. Takahashi[2], Y. Takei[2], A. Fujii[2], C. Hirose[6], T. Iwata[2,11], M. Hayakawa[2], S. Hosoda[2], O. Mori[2], H. Sawada[2], T. Shimada[2], S. Soldini[2], H. Yano[2], R. Tsukizaki[2], M. Ozaki[2,11], Y. Iijima[2‡], K. Ogawa[5], M. Fujimoto[2], T.-M. Ho[26], A. Moussi[27], R. Jaumann[28], J.-P. Bibring[29], C. Krause[30], F. Terui[2], T. Saiki[2], S. Nakazawa[2], Y. Tsuda[2]

Affiliations:

[1]Nagoya University, Nagoya 464-8601, Japan.

[2]Institute of Space and Astronautical Science (ISAS), Japan Aerospace Exploration Agency (JAXA), Sagamihara 252-5210, Japan.

[3]Auburn University, Auburn, AL 36849, USA.

[4]University of Aizu, Aizu-Wakamatsu 965-8580, Japan.

[5]Kobe University, Kobe 657-8501, Japan.

[6]Research and Development Directorate, JAXA, Sagamihara 252-5210, Japan.

[7]University of Tokyo, Tokyo 113-0033, Japan.

[8]Hiroshima University, Higashi-Hiroshima 739-8526, Japan.

[9]Tohoku University, Sendai 980-8578, Japan.

[10]National Astronomical Observatory of Japan, Mitaka 181-8588, Japan.

[11]SOKENDAI (The Graduate University for Advanced Studies), Hayama 240-0193, Japan.

[12]Chiba Institute of Technology, Narashino 275-0016, Japan.

[13]Kindai University, Higashi-Hiroshima 739-2116, Japan.

[14]National Institute of Advanced Industrial Science and Technology, Tokyo 135-0064 Japan.

[15]Kochi University, Kochi 780-8520, Japan.

[16]Rikkyo University, Tokyo 171-8501, Japan.

[17]National Institute of Information and Communications Technology, Kashima 314-8501, Japan.

[18]Università d'Annunzio, 65127 Pescara, Italy.

[19]Seoul National University, Seoul 08826, Korea.

[20]Planetary Science Institute, Tucson, AZ 85710, USA.

[21]Johns Hopkins University Applied Physics Laboratory, Laurel, MD 20723, USA.

[22]Université Côte d'Azur, Observatoire de la Côte d'Azur, CNRS, Laboratoire Lagrange, 06304 Nice, France.

[23]University of Colorado, Boulder, CO 80309, USA.

[24]NASA Johnson Space Center, Houston, TX 77058, USA.

[25]Meiji University, Kawasaki 214-8571, Japan.

[26]DLR (German Aerospace Center), Institute of Space Systems, 28359 Bremen, Germany.

[27]CNES (Centre National d'Etudes Spatiales), 31401 Toulouse, France.

[28]DLR, Institute of Planetary Research, 12489 Berlin-Adlershof, Germany.

[29]Institute d'Astrophysique Spatiale, 91405 Orsay, France.

[30]DLR, Microgravity User Support Center, 51147 Cologne, Germany.

[*]Corresponding author: E-mail: seicoro@eps.nagoya-u.ac.jp

[†]Current affiliation: National Institute for Environmental Studies, Tsukuba 305-8506, Japan.

[††]Current affiliation: Mitsubishi Electric Corporation, Kamakura 247-8520, Japan.

[‡]Deceased.

Abstract: The Hayabusa2 spacecraft arrived at the near-Earth carbonaceous asteroid 162173 Ryugu in 2018. We present Hayabusa2 observations of Ryugu's shape, mass, and geomorphology. Ryugu has an oblate 'spinning top' shape with a prominent circular equatorial ridge. Its bulk density, 1.19 ± 0.03 g cm^{-3}, indicates a high porosity (>50%) interior. Large surface boulders suggest a rubble-pile structure. Surface slope analysis shows Ryugu's shape may have been produced if it once spun at twice the current rate. Coupled with the observed global material homogeneity, this suggests that Ryugu was reshaped by centrifugally induced deformation during a period of rapid rotation.

One Sentence Summary: A proximity survey of Ryugu reveals a rubble-pile carbonaceous asteroid reshaped and homogenized by a past rapid spin.

Main Text:

Carbonaceous (or C-complex) asteroids are leftover debris from planet formation in the solar nebula. Studying their formation, evolution, and volatile content provides information on formation processes around the snow line—the boundary between the inner and outer Solar System (SS).Carbonaceous asteroids may have delivered water and organic materials to the early Earth. The Hayabusa2 mission goal is to rendezvous with an asteroid and probe these issues via a combination of remote-sensing observations from the spacecraft, in-situ surface measurements by deployed rovers and a lander, execution of an artificial impact experiment, and analyses of samples returned to Earth (*1*, *2*). The spacecraft was developed by the Japan Aerospace Exploration Agency (JAXA) as a successor to Hayabusa (*3*) and was launched by an H-IIA

rocket on 3 December 2014. Its target is the near-Earth carbonaceous asteroid 162173 Ryugu (provisional designation 1999 JU_3). Hayabusa2 reached its target in June 2018; NASA's OSIRIS-REx spacecraft(*4*) reached another carbonaceous asteroid 101955 Bennu in December 2018.

After a 3.5-year cruise, a satellite search during approach to the asteroid detected no natural satellites >0.1 m within 100 km [see supplementary text 1 (SM1)]. Hayabusa2 arrived at the Home Position (HP) ~20 km above Ryugu on 27 June 2018. The spacecraft did not enter into circum-asteroid orbit but hovered at HP during the initial mapping phase. The remote-sensing instrument suite onboard Hayabusa2 includes the Optical Navigation Camera - Telescopic (ONC-T) with a wideband and seven narrowband filters (*5*), the Thermal Infrared Imager (TIR) (*6*), a Near-Infrared Spectrometer (NIRS3) (*7*), and a laser Light Detection and Ranging (LIDAR) system (*8*). Coordinated observations among these instruments (Fig. S1, SM1) enabled an initial assessment of Ryugu's general physical characteristics. The spectral data obtained by ONC-T and NIRS3, indicated Ryugu is a Cb-type carbonaceous asteroid with a very low albedo (*5*, *7*).

ONC-T images reveal geomorphological features including the presence of numerous boulders on the surface (Fig. 1). From these images, we constructed global shape models with two independent methods; stereophotoclinometry (SPC) (*9*) and the Structure-from-Motion (SfM) technique (*10*). These methods yielded shape models with polygon mesh resolutions of ~1 m. The two model topographies are in good agreement with each other except for around some boulders and in the polar regions (Fig. S2; SM2). We mainly used the SfM-based shape model (Fig. 2) for further analysis of Ryugu's global shape.

Ryugu's derived orbital and physical parameters are summarized in Table S1 (SM3). The SPC-based shape model provided an estimate of the asteroid spin parameters: an axis with a right ascension of 96.40° ± 0.03°, a declination of −66.40° ± 0.03° at epoch J2000.0 and a period of 7.63262 ± 0.00002 hours. Our derived rotation period is consistent with ground-based observations, while our pole direction fits the second most probable solution compiled from ground- and space-based observations (*11*). The obliquity—the angle between Ryugu's orbital and rotational poles—is 171.64° ± 0.03°, close to perfectly retrograde rotation (which would be at 180°). No wobble or change of the rotation rate have been detected (*12*).

Ryugu has an oblate body with an equatorial radius of 502 ± 2 m and polar to equatorial axes ratio of 0.872 ± 0.007. The total volume obtained from the SPC-based shape model is 0.377 km^3 with an uncertainty of 1.3%. We conducted a gravity measurement (SM3) during a spacecraft ballistic descent down to 0.85 km from the asteroid surface and a subsequent ballistic ascent. The estimated mass is 4.50×10^{11} kg with an uncertainty of 1.3%, mainly due to uncertainties in the solar radiation pressure on the spacecraft. The bulk density is therefore 1.19 ± 0.03 g cm^{-3}, less than the bulk densities (1.6 to 2.4 g cm^{-3}) measured for hydrated carbonaceous asteroids (Ch- and Cgh-type) (*13*). However, it falls within the 0.8–1.5 g cm^{-3} range measured for BCG-types [B-, C-, Cb-, and Cg-type; Ryugu is Cb-type (*5*)], which might be related to unheated icy asteroids (*13*).

NIRS3 observations indicate that OH-bearing minerals are ubiquitous on the surface of Ryugu (*7*). The presence of water ice could explain the low bulk densities of main-belt carbonaceous asteroids, but is unlikely at Ryugu because the radiative equilibrium temperature (~250 K) is higher than the ice sublimation temperature (~230 K) even at its calculated central

pressure of ~8 Pa, and the estimated thermal diffusion time (<10^5 yr) is much shorter than the typical dynamical lifetime of near-Earth asteroids (~10^7 yr) (SM4).

The total porosity is derived to be >50% if the constituent grain density is similar to those of carbonaceous chondrites, of which the lowest known is the 2.42 ± 0.06 g cm^{-3} Orgueil CI meteorite (*14*). The estimated total porosity is slightly higher than the rubble-pile asteroid Itokawa (44 ± 4%) (SM5), suggesting that Ryugu is also a rubble pile, i.e., an aggregate of numerous rocky blocks bound primarily by self-gravity, with low cohesive strength and high bulk porosity. This is consistent the hypothesis that all SS bodies with diameter of ~1 km are rubble piles (*15*). These asteroids might have originally formed from re-accumulation of fragments generated by catastrophic disruption events of ~100-km sized parent bodies (*16*). Ryugu's high porosity could be ascribed to loss of volatile components during or after the formation of the rubble pile, if its parent body was an icy asteroid.

Further evidence for a rubble-pile structure is the abundance of large boulders on the surface. The largest, Otohime, is located near the south pole and ~160 m in its longest axis (Fig. 1). The spatial density of boulders on Ryugu with longest axes >20 m is more than twice that on Itokawa (*5*). Gravitational capture of ejecta after impact cratering on this body cannot be responsible for these large boulders, because their sizes are larger than the ejecta expected from even the largest crater Urashima (~290 m in diameter) (*5*, *17*). These boulders are most likely fragments that accreted during the formation of Ryugu, after disruption of its parent body (*16*).

Little was known about Ryugu's shape prior to Hayabusa2's arrival, due to a lack of radar imaging data and limited constraints from lightcurve observations (*11*). Hayabusa2 images reveal that Ryugu is a spinning-top-shaped asteroid; there is an elevated ridge around the equator, from which near conical surfaces extend to the mid-latitudes, with an average surface tilt angle of 34 ± 4° relative to its spin axis (Figs. 2 and S3, Table S2; SM6). Ryugu's shape is similar to that of Bennu (*4*, *18*). Other spinning-top-shaped near-Earth asteroids have been observed via ground-based radar (Table S3). However, Ryugu's shape was unexpected because its rotation rate is slower than most of the currently known spinning-top-shaped asteroids (*20*).

The aspect ratio of Ryugu's equatorial cross-section is 0.98 and the circularity—the ratio of the circumference of an equal area circle to the perimeter—is 0.93 (Table S3; SM7). This suggests rotation-induced deformation of Ryugu, due to a short spin period (*16*, *21*, *22*). However, the current spin rate is too slow to explain the shape, so Ryugu must have spun faster in the past and later slowed down to its current rate. This deformation hypothesis would also explain surface tilt angles that are symmetric and independent of longitude in the low latitudes (*5*) (SM6). Exceptions are several crater-affected portions, which must have formed after the equatorial ridge.

To constrain the past spin rate that formed the spinning-top shape, we analyzed the distribution of surface slopes—the angle between the normal vector to the surface and that to the surface of equipotential gravitational field—at different spin rates (*18*). Assuming a uniform density distribution, we used the derived bulk density and shape to calculate the surface slope distributions (Fig. 3A) and maps (Fig. 3B). At the current rotation period, the majority of the surface has slopes <35°, but Ryugu exhibits a latitudinal variation; the mid-latitudes have lower slopes while both sides of the equatorial ridge have higher slopes. This results from the surface geopotential that has local maxima in the equatorial and polar regions and becomes lowest at the mid-latitudes (Fig. S4). At a rotation period P_a of 4.0 hours, the local minimum moves to the

equator, while the slopes still have a latitudinal variation (Fig. S5). At $P_a = 3.5$ hours, which is almost equal to the critical spin period at which the centrifugal force exceeds gravity at some surface points near the equator, the surface slope distribution is centered at $31°^{+14°}_{-11°}$ (Fig. 3A). This distribution is consistent with a typical friction angle of granular materials (~35°) [e.g., (*23*)], suggesting topographic relaxation that homogenized the slope distribution (*5*). During this process, the variation in surface slopes minimizes at low- and mid-latitudes (Figs. 3A and B, S5) as a result of a deformation process that produced the equatorial ridge (*15*, *18*).

Geological features of the equatorial ridge (*5*) are: (i) large unperturbed craters overlying the ridge, suggesting the ridge formed before the craters, (ii) imbricated boulders indicating surface mass wasting from the equator to the mid-latitudes, (iii) no evidence of grain-size segregation, unlike Itokawa (*3*), suggesting a lower degree of global surface activity. Candidate structural lineaments have been found around the equatorial region, but we regard them as unconfirmed due to limited lighting conditions in available high resolution images.

To determine the material properties of the equatorial ridge, we analyzed observation data acquired for the purpose of evaluating candidate sample collection sites: four (L sites) on the equatorial ridge and three (M sites) at higher latitudes (15° to 30°) (Fig. S6, Table S4; SM8). Each candidate region has a size of 14° by 14° (about 110 by 110 m^2), which were targeted for detailed investigation. The variation between these regions in the visible and NIR reflectance data is less than 15%, suggesting efficient mixing processes in the surface layer (*5*, *7*). Within this limited spectral variation, a difference was found in ONC-T data on the spectral slope γ between the b- and x-bands (0.48 to 0.86 μm) (*5*) (SM9). High-resolution maps of γ at candidate sampling sites reveal that bluish and reddish materials are mixed in different degrees (Fig. 4A). The slope γ was found to correlate with the v-band reflectance factor r_v (*5*). The sites along the equatorial ridge (L-sites) have brighter bluish spectra, whereas those in higher latitudes (M-sites), especially M01, exhibit darker reddish spectra (Fig. 4B). The trend of r_v with γ may be ascribed to the effect of space exposure on fresh bright-blue materials leading to reddening and darkening (*5*). Thus, mass wasting after spin down of Ryugu probably exposed fresh subsurface materials on the equatorial ridge.

Our current observations are insufficient to identify when and how the spinning-top shape formed. Possible timings are either an early re-accumulation stage after catastrophic disruption of Ryugu's parent body (*16*) and/or a later stage due to quasi-static rotational acceleration (*21*, *22*). Early stage formation may explain the presence of large craters on the equatorial ridge. However, the conditions for producing a spinning-top shape are unclear, because Ryugu would need to gain a high enough angular momentum during re-accumulation to produce its axisymmetric shape and circular ridge, but avoid a non-axisymmetric instability that makes the shape elongated.

In the later stage the Yarkovsky-O'Keefe-Radzievskii-Paddack (YORP) effect, a radiation recoil torque affecting the rotation state of a small asteroid, is responsible for the quasi-static acceleration of asteroids [e.g., (*15*)]. When a spheroidal asteroid spins rapidly, strong centrifugal forces may induce deformation processes either on the surface (*21*, *24*) or in the interior (*25*, *26*), depending on the internal structure (*26*, *27*). The large porosity of Ryugu, the dominance of large grains (>1 cm) across its surface (*5*), and the lack of observed benches in its

largest craters (*5*) suggest that the internal cohesive strength of the asteroid may be uniform and low.

Given the bulk density, shape, and uniform structure, we calculated the failure mode of Ryugu by using a plastic finite element model (FEM) technique (*20*) (SM10). This FEM method models continuum media to describe irreversible deformation of the regolith in asteroids. If Ryugu rotates at $P_a < 3.75$ hours, tension plays a dominant role in deformation in the interior (Fig. S7). At $P_a = 3.5$ hours, the first structural failure occurs in the central region (Fig. 3C) if the cohesive strength (*28*) is uniformly ~4 Pa, which is similar to the predicted cohesive strength of small bodies (*22*, *25*). While the van der Waals force may contribute to cohesion (*22*), density inhomogeneity or particle interlocking may also produce equivalent mechanical strength. The failed region spreads over the interior, driving outward, radial deformation parallel to the equatorial plane and inward, vertical deformation around the spin axis (Fig. 3C). This model may support a lower degree of global surface activity on Ryugu (*5*). However, we do not rule out contributions from surface landslides to spinning-top-shape formation (*26*), which can be driven by local heterogeneities (*12*) or a gradual increase in strength of the asteroid with depth. These scenarios predict differing freshness of the subsurface material beneath the equatorial ridge due to the time available for space weathering. .

References and Notes:

1. S. Tachibana *et al.*, Hayabusa2: Scientific importance of samples returned from C-type near-Earth asteroid (162173) 1999 JU3. *Geochem. J.* **48**, 571–587 (2014). doi: 10.2343/geochemj.2.0350
2. S. Watanabe *et al.*, Hayabusa2 mission overview. *Space Sci. Rev.* **208**, 3–16 (2017). doi: 10.1007/s11214-017-0377-1
3. A. Fujiwara *et al.*, The rubble-pile asteroid Itokawa as observed by Hayabusa. *Science* **312**, 1330–1334 (2006). doi: 10.1126/science.1125841
4. D. S. Lauretta *et al.*, OSIRIS-REx: Sample return from asteroid (101955) Bennu. *Space Sci. Rev.* **212**, 925–984 (2017). doi: 10.1007/s11214-017-0405-1
5. S. Sugita *et al.*, The geomorphology, color, and thermal properties of Ryugu: Implications for parent-body processes. *Science*, this issue
6. T. Okada *et al.*, Thermal infrared imaging experiments of C-type asteroid 162173 Ryugu on Hayabusa2. *Space Sci. Rev.* **208**, 255–286 (2017). doi: 10.1007/s11214-016-0286-8
7. K. Kitazato *et al.*, Surface composition of asteroid 162173 Ryugu as observed by the Hayabusa2 NIRS3 instrument. *Science*, this issue
8. T. Mizuno *et al.*, Development of the Laser Altimeter (LIDAR) for Hayabusa2. *Space Sci. Rev.* **208**, 33–47 (2017). doi: 10.1007/s11214-015-0231-2
9. R. W. Gaskell et al., Characterizing and navigating small bodies with imaging data. *Meteorit. Planet. Sci.* **43**, 1049–1061 (2008). doi: 10.1111/j.1945-5100.2008.tb00692.x
10. R. Szeliski, *Computer Vision: Algorithms and Applications* (Science & Business Media, Springer, New York, 2010).

11. T. G. Müller *et al.*, Hayabusa-2 mission target asteroid 162173 Ryugu (1999 JU3): Searching for the object's spin-axis orientation. *Astron. Astrophys.* **599**, A103 (2017). doi: 10.1051/0004-6361/201629134

12. A small deviation (0.7° to 0.8°) of the principal axis of inertia from the spin axis was obtained, considering the shape models and assuming uniform density distribution (SM2).

13. P. Vernazza *et al.*, Interplanetary dust particles as samples of icy asteroids. *Astrophys. J.* **806**, 204 (2015). doi: 10.1088/0004-637X/806/2/204

14. R. J. Macke, G. J. Consolmagno, D. T. Britt, Density, porosity, and magnetic susceptibility of carbonaceous chondrites. *Meteorit. Planet. Sci.* **46**, 1842–1862 (2011). doi: 10.1111/j.1945-5100.2011.01298.x

15. K. J. Walsh, Rubble pile asteroids. *Ann. Rev. Astron. Astrophys* **56**, 593–624 (2018). doi: 10.1146/annurev-astro-081817-052013

16. P. Michel, W. Benz, P. Tanga, D. C. Richardson, Collisions and gravitational reaccumulation: Forming asteroid families and satellites. *Science* **294**, 1696–1700 (2001). doi: 10.1126/science.1065189

17. T. Michikami *et al.*, Size-frequency statistics of boulders on global surface of asteroid 25143 Itokawa. *Earth Planet. Space* **60**, 13–20 (2008). doi: 10.1186/BF03352757

18. D. J. Scheeres *et al.*, The geophysical environment of Bennu. *Icarus* **276**, 116–140 (2016). doi: 10.1016/j.icarus.2016.04.013

19. Y. Yu *et al.*, The dynamical complexity of surface mass shedding from a top-shaped asteroid near the critical spin limit. *Astron. J.* **156**, 59 (2018). doi: 10.3847/1538-3881/aaccf7

20. M. Hirabayashi, D. J. Scheeres, Rotationally induced failure of irregularly shaped asteroids. *Icarus* **317**, 354–364 (2019). doi: 10.1016/j.icarus.2018.08.003

21. K. J. Walsh, D. C. Richardson, P. Michel, Rotational breakup as the origin of small binary asteroids. *Nature* **454**, 188–191 (2008). doi: 10.1038/nature07078

22. P. Sánchez, D. J. Scheeres, Disruption patterns of rotating self-gravitating aggregates: A survey on angle of friction and tensile strength. *Icarus* **271**, 453–471 (2016). doi: 10.1016/j.icarus.2016.01.016

23. T. W. Lambe, R. V. Whitman, *Soil Mechanics* (Series in Soil Engineering, Wiley, Hoboken, NJ, 1969).

24. D. J. Scheeres, Landslides and Mass shedding on spinning spheroidal asteroids. *Icarus* **247**, 1–17 (2015). doi: 10.1016/j.icarus.2014.09.017

25. M. Hirabayashi, D. J. Scheeres, Stress and failure analysis of rapidly rotating asteroid (29075) 1950 DA. *Astrophys J. Lett.* **798**, L8 (2014). doi: 10.1088/2041-8205/798/1/L8

26. M. Hirabayashi, D. P. Sánchez, D. J. Scheeres, Internal structure of asteroids having surface shedding due to rotational instability. *Astrophys. J.* **808**, 63 (2015). doi: 10.1088/0004-637X/808/1/63

27. Y. Zhang *et al.*, Rotational failure of rubble-pile bodies: Influences of shear and cohesive strengths. *Astrophys. J.* **857**, 15 (2018). doi: 10.3847/1538-4357/aab5b2

28. The cohesive strength σ_c of Ryugu-formed aggregates is given by $\sigma_c = \sigma_t \tan\theta$, where σ_t and θ are the tensile strength and the angle of friction of the aggregates, respectively.

29. R. Jaumann *et al.*, The camera of the MASCOT asteroid lander on board Hayabusa 2. *Space Sci. Rev.* **208**, 375–400 (2017). doi: 10.1007/s11214-016-0263-2

30. J.-P. Bibring *et al.*, The MicrOmega investigation onboard Hayabusa2. *Space Sci. Rev.* **208**, 401–412 (2017). doi: 10.1007/s11214-017-0335-y

31. S. Kameda *et al.*, Preflight calibration test results for optical navigation camera telescope (ONC-T) onboard the Hayabusa2 spacecraft. *Space Sci. Rev.* **208**, 17–31 (2017). doi: 10.1007/s11214-015-0227-y

32. F. Mignard, Radiation pressure and dust particle dynamics. *Icarus* **49**, 347–366 (1982). doi: 10.1016/0019-1035(82)90041-0

33. D. P. Hamilton, J. A. Burns, Orbital stability zones about asteroids: II. The destabilizing effects of eccentric orbits and of solar radiation. *Icarus* **96**, 43–64 (1992). doi: 10.1016/0019-1035(92)90005-R

34. K. Wada *et al.*, Asteroid Ryugu before the Hayabusa2 encounter. *Prog. Earth Planet. Sci.* **5**, 82, (2018). doi: 10.1186/s40645-018-0237-y

35. J. D. Giorgini, "NASA JPL Horizons On-Line Ephemeris System", (2015; http://ssd.jpl.nasa.gov/?horizons).

36. W. M. Folkner, J. G. Williams, D. H. Boggs, R. S. Park, P. Kuchynka, "The planetary and lunar ephemerides DE430 and DE431" (Interplanetary Network Progress Rep. 42–196, Jet Propulsion Lab., 2014).

37. B. G. Marsden, Z. Sekanina, D. K. Yeomans, Comets and nongravitational forces. V. *Astron. J.*, **78**, 211–225 (1973). doi: 10.1086/111402

38. Y. Tsuda, M. Yoshikawa, M. Abe, H. Minamino, S. Nakazawa, System design of the Hayabusa2—Asteroid sample return mission to 1999 JU3. *Acta Astronautica* **91**, 356–362 (2013). doi: 10.1016/j.actaastro.2013.06.028

39. T. Kominato, M. Matsuoka, M. Uo, T. Hashimoto, J. Kawaguchi, Optical hybrid navigation and station keeping around Itokawa. AIAA/AAS Astrodynamics Specialist Conference and Exhibit, Keystone, CO, 23 August 2006. doi: 10.2514/6.2006-6535

40. F. Terui *et al.*, "GN&C of Hayabusa2 in cruising phase and asteroid proximity phase" in *Guidance, Navigation, and Control 2016*, D. A. Chart. Ed. (Advances in the Astronautical Sciences Series **157**, Univelt, San Diego, 2016), pp. 667–678 (AAS 16-106).

41. H. Morita, K. Shirakawa, T. Kubota, T. Hashimoto, J. Kawaguchi, Hayabusa's real-time landmark tracking navigation for descents and touching-downs. AIAA/AAS Astrodynamics Specialist Conference and Exhibit, Keystone, CO, 23 August 2006. doi: 10.2514/6.2006-6537

42. N. Sakatani, K. Ogawa, M. Arakawa, S. Tanaka, Thermal conductivity of lunar regolith simulant JSC-1A under vacuum. *Icarus* **309**, 13–24 (2018). doi: 10.1016/j.icarus.2018.02.027

43. G. J. Consolmagno *et al.*, The measurement of meteorite heat capacity at low temperatures using liquid nitrogen vaporization. *Planet. Space Sci.* **87**, 146–156 (2013). doi: 10.1016/j.pss.2013.07.009

44. B. Gladman, P. Michel, Ch. Froeschlé, The near-Earth object population. *Icarus* **146**, 176–189 (2000). doi: 10.1006/icar.2000.6391

45. A. Tsuchiyama *et al.*, Three-dimensional structure of Hayabusa samples: Origin and evolution of Itokawa regolith. *Science* **333**, 1125–1128 (2011). doi: 10.1126/science.1207807

46. R. A. Werner, D. J. Scheeres, Exterior gravitation of a polyhedron derived and compared with harmonic and mascon gravitation representations of asteroid 4769 Castalia. *Celest. Mech. Dyn. Astron.* **65**, 313–344 (1996). doi: 10.1007/bf00053511

47. E. G. Kahn *et al.*, A tool for the visualization of small body data. *Proc. Lunar Planet. Sci. Conf.* **43**, abstr. 1618 (2011).

48. C. A. Schneider, W. S. Rasband, K. W. Eliceiri, NIH Image to ImageJ: 25 years of image analysis. *Nature Methods* **9**, 671–675 (2012). pmid: 22930834

49. A. K. Mainzer *et al.*, "NEOWISE diameters and albedos V1.0" (EAR-A-COMPIL-5-NEOWISEDIAM-V1.0, NASA Planet. Data Syst., 2016).

50. M. W. Busch *et al.*, Physical modeling of near-Earth Asteroid (29075) 1950 DA. *Icarus* **190**, 608–621 (2007). doi: 10.1016/j.icarus.2007.03.032

51. M. W. Busch *et al.*, A. A. Hine, Physical properties of near-Earth Asteroid (33342) 1998 WT24. *Icarus* **195**, 614–621 (2008). doi: 10.1016/j.icarus.2008.01.020

52. S. J. Ostro *et al.*, Radar imaging of binary near-Earth asteroid (66391) 1999 KW4. *Science* **314**, 1276–1280 (2006). doi: 10.1126/science.1133622

53. M. W. Busch *et al.*, Radar observations and the shape of near-Earth Asteroid 2008 EV5. *Icarus* **212**, 649–660 (2011). doi: 10.1016/j.icarus.2011.01.013

54. M. C. Nolan *et al.*, "Asteroid (101955) Bennu Shape Model V1.0" (EAR-A-I0037-5-BENNUSHAPE-V1.0, NASA Planet. Data Syst., 2013).

55. E. Tatsumi *et al.*, Updated inflight calibration of Hayabusa2's Optical Navigation Camera (ONC) for scientific observations during the cruise phase. https://arxiv.org/abs/1810.11065 (2018).

56. B. Hapke, Bidirectional reflectance spectroscopy: 4. The extinction coefficient and the opposition effect. *Icarus* **67**, 264–280 (1986). doi: 10.1016/0019-1035(86)90108-9

57. M. Ishiguro *et al.*, Optical properties of (162173) 1999 JU3: In preparation for the JAXA Hayabusa 2 sample return mission. *Astrophys. J.* **792**, 74–82 (2014). doi: 10.1088/0004-637X/792/1/74

58. H. Si, 2015, TetGen, a delaunay-based quality tetrahedral mesh generator. *ACM Transactions on Mathematical Software* **41**, 11 (2015). doi: 10.1145/2629697

Acknowledgments: The Hayabusa2 spacecraft was developed and built under the leadership of JAXA, with contributions from the German Aerospace Center (DLR) and the Centre

National d'Études Spatiales (CNES), and in collaboration with Nagoya University, University of Tokyo, National Astronomical Observatory of Japan, University of Aizu, Kobe University, and other universities, institutes, and companies in Japan. We thank NASA, DSN, and JPL for their support for the execution of the Hayabusa2 mission and Hayabusa2 Joint Science Team members for fruitful science discussions. We also thank the many engineers who have contributed to the success of the Hayabusa2 mission, especially Tetsuya Masuda, Seiji Yasuda, Kouta Matsushima, and Takeshi Ohshima at NEC Corporation. S.W. thanks to Carolyn M. Ernst for her support of the development of the SPC-based shape model. T.N. thanks to Kana Amano, Hikari Mita, and Shiho Kobayashi for their support of the LSS process. M.Hi. acknowledges the use of ANSYS Mechanical APDL (18.1), which is licensed by Samuel Ginn College of Engineering at Auburn University. **Funding:** This study was supported by KAKENHI from the Japan Society for the Promotion of Science (JSPS) (Grant Nos. JP17H06459, JP17K05639, JP16H04059, JP17KK0097, JP26287108, JP16H04044) and the JSPS Core-to-Core program "International Network of Planetary Sciences". P.M. acknowledges funding support from the French space agency CNES. **Author contributions:** Conceptualization: S.W., M.Hi., N.H. (Aizu), Y.Ii; Spacecraft operation and data acquisition: M.Yo, S.Ki., H.T., T.O., M.Ab., Y.Ya. S.Tan. (JAXA), K.S., M.Ya, T.Y., N.O., G.O., Y.M., K.Yoshik., T.T., Y.Ta., A.F., C.Hi, T.I., M.Ha., S.H., O.M., H.Sa., T.Sh., S.So., H.Yan., R.T., M.O., K.O., F.T., T.Sa., S.N., Y.Ts.; Analysis (shape models): S.W., M.Hi., N.H. (Aizu), N.H. (Kobe), R.N., Y.S., Y.Is, K.M., H.T., S.Su., R.G., E.P., O.S.B., Y.Ya, S.Tan (Kobe), N.Ni., T.Su., T.Y.; Analysis (gravity): H.I., M.Yo., H.T., A.S.F., J.M.W., D.J.S., Y.M., K.Yosik., S.So., Y.Ts.; Analysis (LSS) S.W. E.T., S.Ki., H.Yab., T.N., S.Tac., Y.Is., T.Mo., K.K., N.S., K.M., K.W., H.Se., C.Ho., T.Mi., H.T., T.K., R.Ho., S.Ka., T.F., H.M., G.K., I.M. P.M., P.A.A., S.Tan. (JAXA), M.M., Y.Yo., H.Su., K.Yoshio., Y.C., H.K., R.He.; Project administration: S.W., M.Yo., S.Tac., K.K., S.Su., T.O., N.Na., M.Ar, M.Ab., S.T. (JAXA), M.F., T.-M. H., A.M., R.J., J.-P. B., C.K., F.T., T.Sa., S.N., Y.Ts.; Writing: S.W., M.Hi., N.H. (Aizu), R.N., Y.S., H.I., E.T., S.Ki., T.N., S.Tac., K.W., H.T., T.K., G.K., O.S.B., P.M., D.J.S., P.A.A., S.So. All authors discussed the results and commented on the manuscript. **Competing interests:** The authors declare no competing interests. **Data and materials availability:** The Hayabusa2 ONC and shape model data will be made available through the JAXA Data Archives and Transmission System website (https://www.darts.isas.jaxa.jp/) and is available upon request until posted to the archive.

Supplementary Materials:

Materials and Methods

Figs. S1 to S7

Tables S1 to S4

References (*31*)–(*58*)

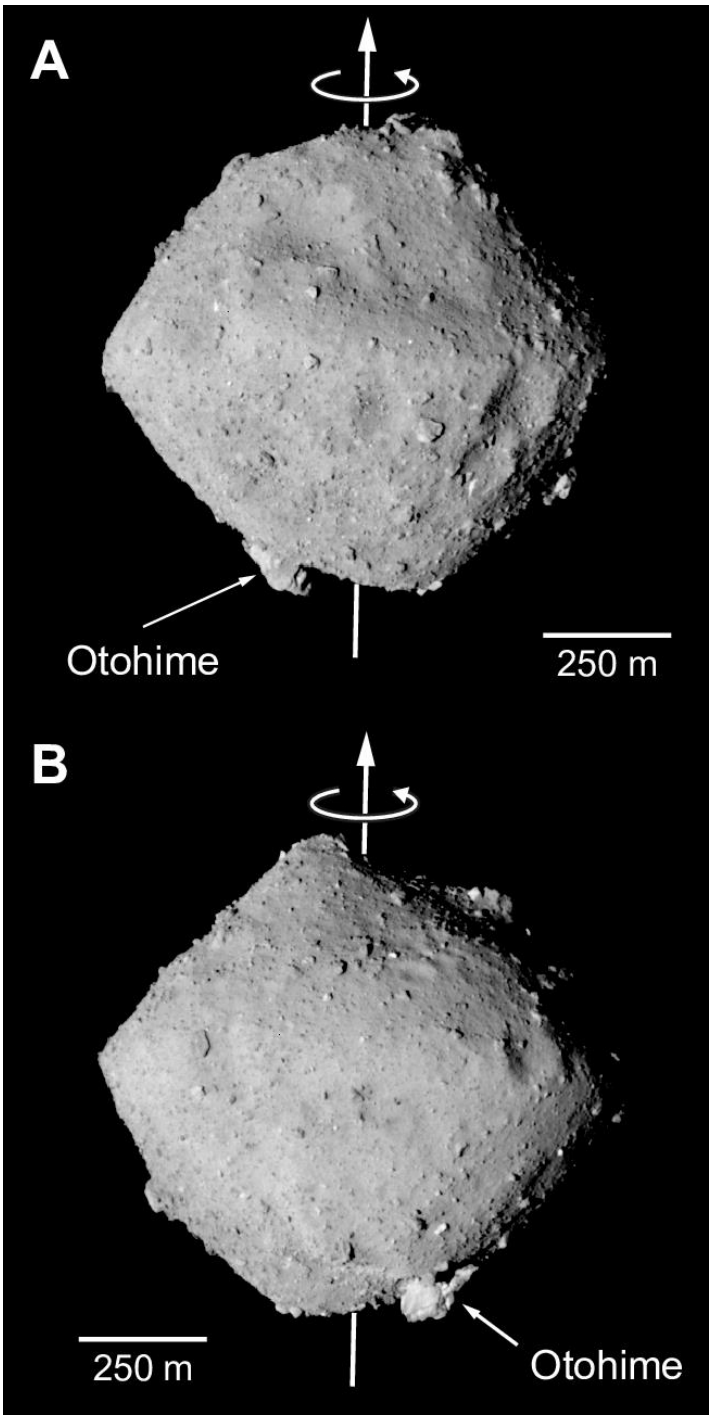

Fig. 1. ONC-T images of Ryugu. Taken from 20 km altitude on 10 July 2018. White arrows represent the spin axis. The prime meridian is defined in (*5*). **(Top)** Hemisphere centered at (5°S, 11°E). **(Bottom)** Hemisphere centered at (5°S, 189°E).

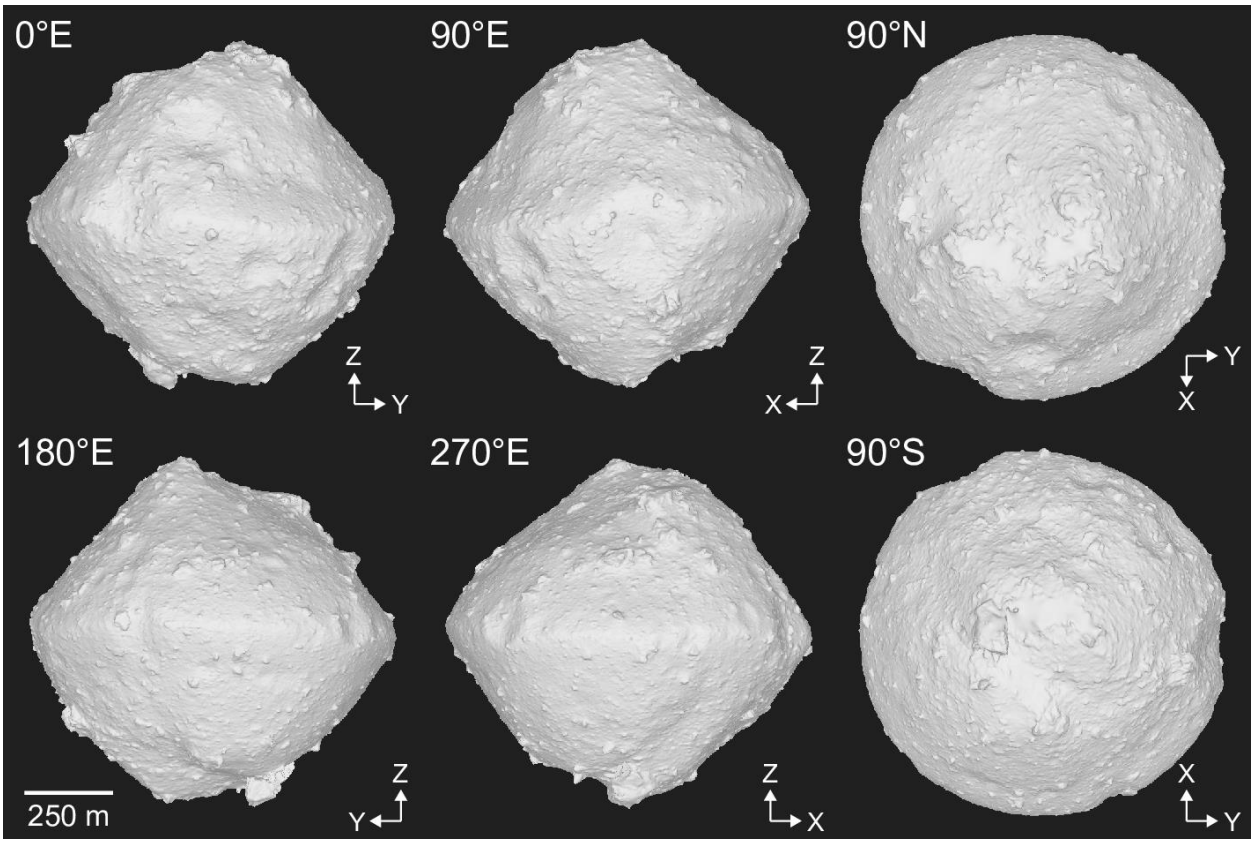

Fig. 2. SfM-based shape model of Ryugu. Generating a polygon model with 3,145,728 facets based on total 214 ONC-T images taken from the 5.1- and 6.5-km altitudes.

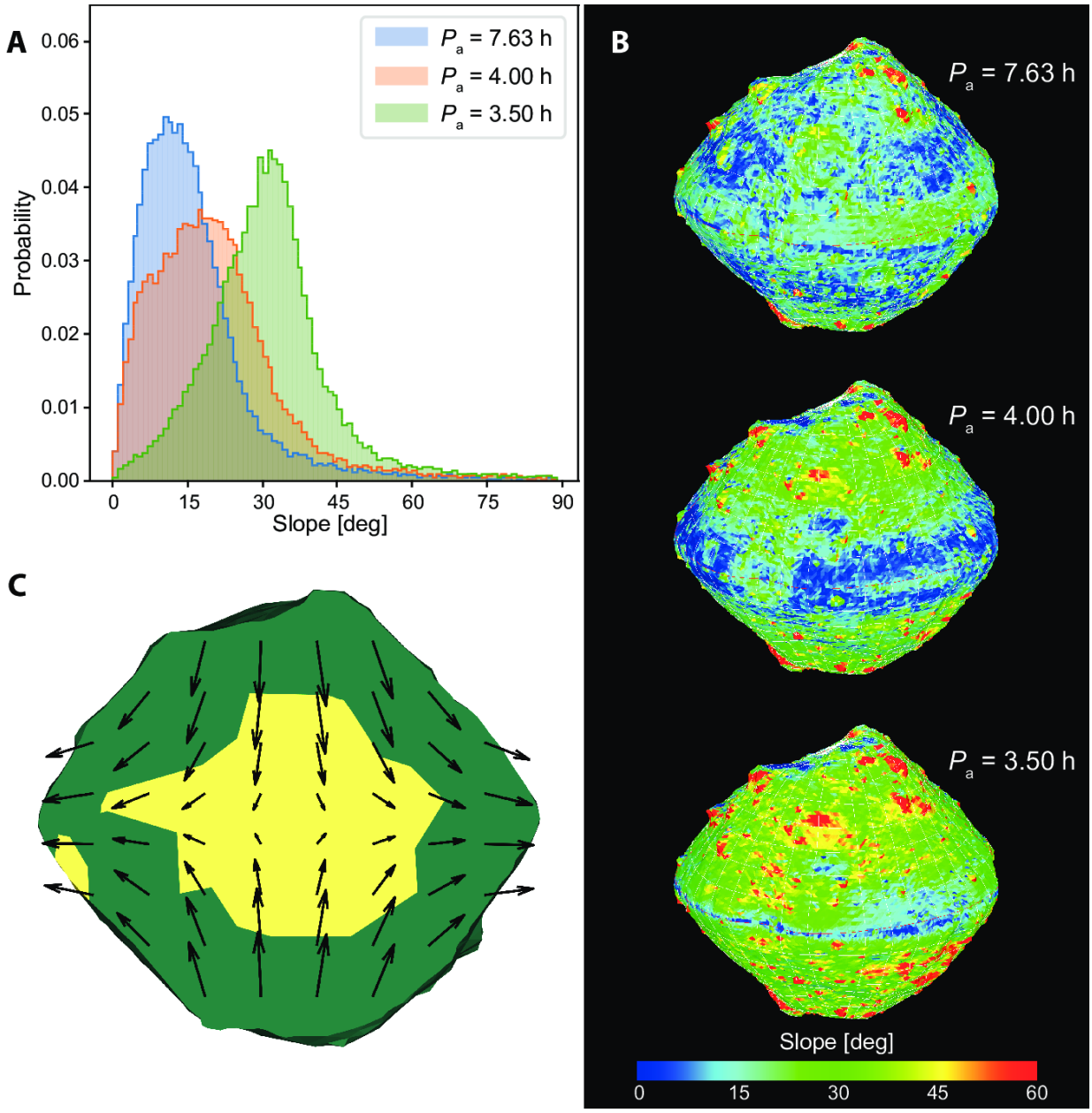

Fig. 3. Slope distribution and failure mode analysis. Reduced versions of SfM- (A, B: 49,152 facets) and SPC-based (C: 3,072 facets) shape models were used. The density is assumed to be constant at 1.2 g cm^{-3}. **(A)** Area-weighted slope distribution at spin periods of 7.63, 4.0, and 3.5 hours. **(B)** Slope maps projected on the shape model at different spin periods. **(C)** Failed region (yellow) and deformation vectors on the meridional cross-section viewed from a longitude of 30°E at a spin period of 3.5 hours. The minimum cohesive strength to keep the original shape is ~4 Pa.

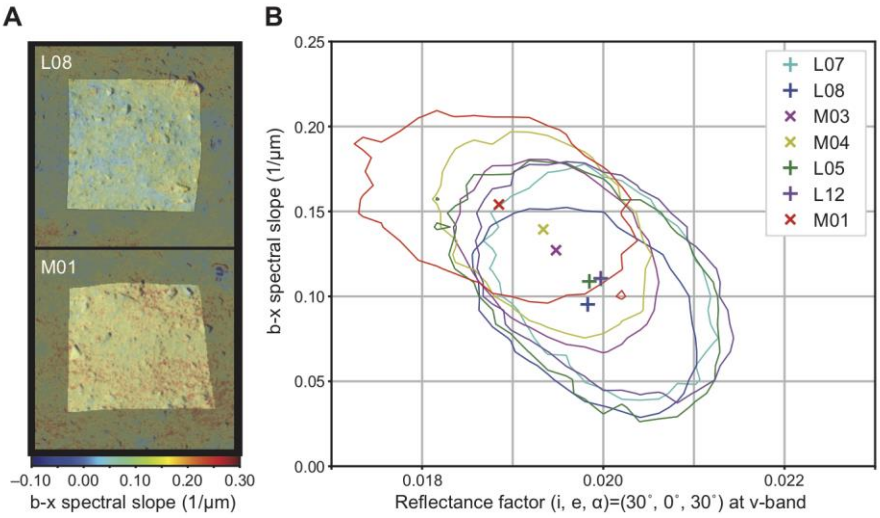

Fig. 4. Visible spectral properties of candidate sampling sites. In accordance with a safety index (SM8) the Hayabusa2 engineering team chose seven candidate sampling sites, L05, L07, L08, L12, M01, M03, and M04, where L and M indicate low-latitude and "mid"-latitude (15° to 30°) regions, respectively. **(A)** ONC-T v-band images of two representative candidate sites, L08 (top) and M01 (bottom), from altitude of ~5 km, overlaid by color maps of b-x (0.48 to 0.86 μm) spectral slope. **(B)** Spectral slope and reflectance factor at v-band of 7 candidate landing sites. Symbols (L: +, M: ×) and lines are showing the median values and 1-σ variations inside those sites, respectively (SM9).